ELSEVIER

Nuclear Physics B 434 (1995) 503–532

NUCLEAR PHYSICS B

# Search for neutrino oscillations at 15, 40 and 95 meters from a nuclear power reactor at Bugey

B. Achkar [a], R. Aleksan [b], M. Avenier [a], G. Bagieu [a], J. Bouchez [b], R. Brissot [a], J.-F. Cavaignac [a], J. Collot [a], M-C. Cousinou [c], J.P. Cussonneau [d], Y. Declais [e], Y. Dufour [d], J. Favier [e], F. Garciaz [c], E. Kajfasz [c], H. de Kerret [d], D.H. Koang [a], B. Lefièvre [d], E. Lesquoy [b], J. Mallet [b], A. Metref [e], E. Nagy [c], H. Pessard [e], F. Pierre [b] M. Obolensky [d], A. Stutz [a], J.P. Wuthrick [d,1]

[a] *Institut des Sciences Nucléaires, IN2P3-CNRS, F-38026 Grenoble, CEDEX, France*

[b] *CEA, DAPNIA, Service de Physique des Particules, CE Saclay, F-91191 Gif-sur-Yvette, CEDEX, France*

[c] *Centre de Physique des Particules de Marseille, Faculté des Sciences de Luminy, IN2P3-CNRS, F-91288 Marseille, CEDEX 09 France*

[d] *Collège de France, Laboratoire de Physique Corpusculaire, IN2P3-CNRS, F-75231 Paris, CEDEX 05, France*

[e] *Laboratoire d'Annecy-le-Vieux de Physique des Particules, LAPP, IN2P3-CNRS, BP 110, F-74941 Annecy-le-Vieux, CEDEX, France*

Received 19 October 1994; revised 3 November 1994; accepted 10 November 1994

**Abstract**

We report on high statistics measurements of neutrino energy spectra carried out at 15, 40 and 95 meters from a 2800 Megawatt reactor, using detection modules filled with $^6$Li-loaded liquid scintillator. No oscillations have been observed. Exclusion zones for oscillation parameters are deduced from the observed consistency of the spectra at the three distances. The minimum excluded values of the $\delta m^2$ and $\sin^2 2\theta$ parameters are $1 \times 10^{-2}$ eV$^2$ and $2 \times 10^{-2}$ (at 90% CL), respectively.

[1] Deceased.


*SSDI* 0550-3213(94)00513-3

## 1. Introduction

Searching for neutrino oscillations provides an elegant tool to study physics beyond the Standard Model [1]. Indeed, if neutrino oscillations exist, at least one of the neutrinos should have a mass and the different lepton families should mix together. Neither of these two phenomena are expected in the Standard Model.

Nuclear power reactors are the most intense sources of anti-neutrinos available on Earth ($5 \times 10^{20} \bar{\nu}_e$ per second for 2800 MW reactors). Neutrino oscillations can be studied near a reactor by looking for a variation of the observed flux and spectrum with distance (disappearance method). As is well known [2], in the case of two neutrino mixing the probability $P$ for the originally missing flavour to appear is proportional to the mixing parameter, $\sin^2 2\theta$:

$$P = \sin^2 2\theta \cdot \sin^2 \left( \frac{1.27 \cdot \delta m^2 \cdot l}{E_\nu} \right), \tag{1}$$

where $E_\nu$ is the neutrino energy (in MeV), $l$ is the distance (in $m$) between the production and the detection of the neutrino and $\delta m^2$ is the difference of the masses squared (in $\mathrm{eV}^2$) between the two neutrino mass-eigenstates. Due to the low energies of these neutrinos (a few MeV), experiments at reactors are sensitive to lower mass differences ($\approx 10^{-2}\mathrm{eV}^2$ for distances of a few tens of meters) than experiments at accelerators. On the other hand, accelerator experiments which compare $P$ directly to the data (appearance method) are more sensitive to small values of the mixing parameter than the reactor experiments, where $1 - P$ is measured.

The Bugey nuclear power plant runs four Pressurized Water Reactors (PWR) of 2800 thermal MW each. A first experiment performed at 14 and 18 meters from one of the reactors and completed in 1984 [3] had shown a decrease in the number of neutrino events between the two distances, which had been interpreted as an indication for neutrino oscillation. This effect was not confirmed by a remeasurement performed in 1986 after modifications of the detector shielding which led to a strong decrease of the cosmic ray induced neutron background [4]. We present here a new measurement performed at 15, 40 and 95 meters using a different, novel neutron detection technique. Three identical modules have been used: one (module 1) located under the reactor building, at 15 meters from the core, and two (module 2 and module 3) outside the reactor building, inside a concrete bunker 40 meters away from the core. The data taken with module 1 were also used to extract the neutrino signal from another reactor located at 95 meters when the nearest one was stopped. The statistical accuracy was significantly improved, we have recorded about 150000 events, the highest number of electron anti-neutrinos ever detected. In addition, in about 40% of the whole data taking period we have carried out the measurements *simultaneously* at the two locations. This has the advantage, when comparing data at two distances, of being less sensitive to the modification of the source spectrum due to the evolution with time of the fuel composition (the so called burn-up effect) which is a source of systematic uncertainties. Preliminary results have been reported earlier [5,6].

## 2. The detection principle

We detect $\bar{\nu}_e$'s by their charged current interaction

$$\bar{\nu}_e + p \longrightarrow e^+ + n \tag{2}$$

on the free protons of the target which is a pseudocumene based liquid scintillator with an H/C ratio of 1.4 doped with 0.15% in mass of $^6$Li [7]. The signature of such an event is

–a prompt light pulse from the positron which can be related through the response function of the detector to the positron kinetic energy, $E_{e^+}$ and thus the neutrino energy:

$$E_{\bar{\nu}} \simeq E_{e^+} + 1.8\,\text{MeV}, \tag{3}$$

–a delayed (by 30 $\mu$s on average) light pulse due to the produced neutron which is thermalized and captured with high probability by the $^6$Li nuclei in the liquid:

$$n + {}^6\text{Li} \longrightarrow {}^4\text{He} + {}^3\text{H} + 4.8\,\text{MeV}. \tag{4}$$

Because of the strong quenching coefficient of the scintillator, the 4.8 MeV peak is seen as a 0.530 MeV peak in equivalent electron energy [8]. This peak is the first evidence of the presence of a neutron. Additional evidence is obtained by the good pulse shape discrimination (PSD) property of the scintillator [9,10]. As shown in Fig. 1, the quantity

$$R_{\text{PSD}} = \frac{\text{delayed charge}}{\text{total charge}} \tag{5}$$

can be used with good efficiency to distinguish heavy particles (alphas, tritium or slow protons) from electrons for the same total number of photoelectrons. This PSD property is also used to distinguish the positron in reaction (2) from recoil protons produced by fast cosmic neutrons.

The neutron capture time (30$\mu$s) and its mean free path (6 cm) allow efficient reduction of the accidental background by performing delayed time coincidence between the neutron and the positron signals as well as by requiring spatial proximity between them making use of the segmentation of the detector. The main components of the accidental background are Compton electrons produced by low energy gammas and alpha particles from internal radioactivity of the scintillator. Special care had to be taken to decrease this activity associated with the uranium contamination of the lithium salt. Unfortunately, however, a new liquid with purer $^6$Li component showed a chemical instability leading to a $\approx$ 1% daily loss of detected light except for one batch where the loss was acceptable (4% per month) [8]. This batch was used in the 15 meter position. At 40 meters the liquid used was chemically stable but the alpha radioactivity gave $\sim$ 2 times more random coincidences in the final analysis than at the 15 meter position.

## 3. The detector

The detector and its performance will be described in detail elsewhere [8]. We give here the main characteristics. A schematic view of one detector module is shown in

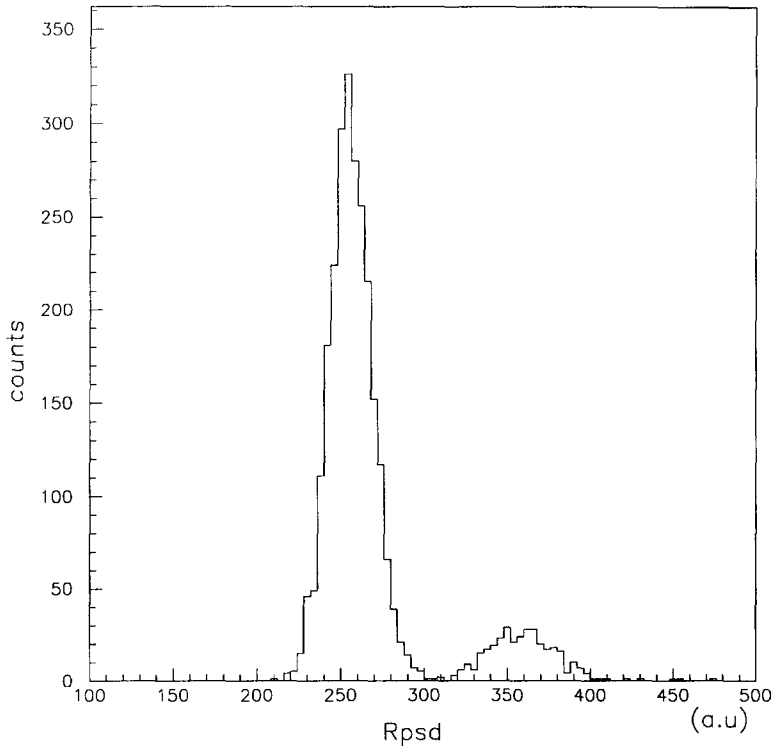


Fig. 1. Distribution of the $R_{PSD}$ ratio obtained using an Am–Be source: the peak at low $R_{PSD}$ value is due to Compton electrons, the one at high $R_{PSD}$ value is due to recoil protons at the $e^-$ equivalent energy of 4.3 MeV.

Fig. 2 together with the principle of the detection of the neutrinos.

Each detection module is a $\sim$ 600 liter[2] stainless steel tank of $85 \times 122.5 \times 61.8$ cm$^3$ internal dimensions and with two acrylic windows (0.8 cm thick) on two opposite faces to collect the scintillation light. This tank is optically segmented in 98 ($7 \times 14$) elementary cells ($8.5 \times 8.5 \times 85.0$ cm$^3$), separated by walls made of a 150 $\mu$m thick steel foil, covered with an aluminium foil and separated from the liquid by transparent thermosealed FEP teflon, 125 $\mu$m thick, with a nitrogen gas gap maintained by spacers between the teflon and aluminium for optimal light reflection. Each cell is seen on each side by a 3-inch photomultiplier RTC XP 3462. We obtained 150 photoelectrons per MeV with such a light-collection system. Comparisons of pulse heights on opposite PMT's allowed for a localization of the light emission point along the cell ($z$ direction).

The module(s) at 15 (40) meters is (are) installed inside a shielding made of successive layers consisting of, from outside inwards, 10 cm of lead (15 cm of iron) to stop gammas, 25 cm of water followed by 4 mm $B_4C$ to slow down and capture

[2] At the 40 m position one of the modules was filled up only to the 6/7th of its total volume.

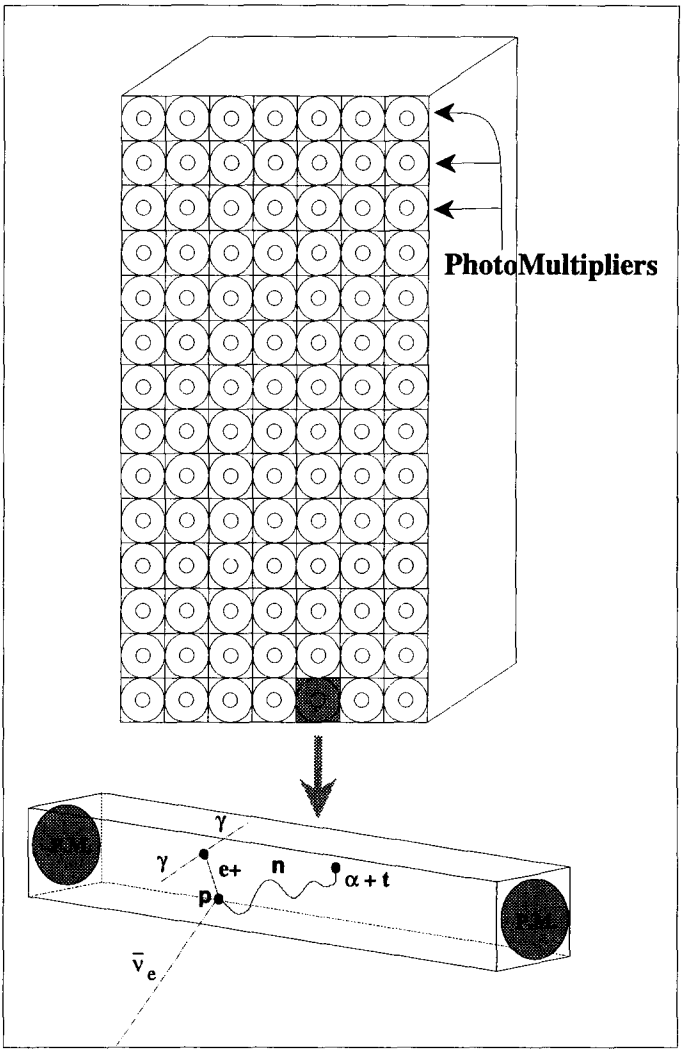


Fig. 2. The schematic view of one detector module.

fast neutrons, and finally 8 cm of liquid scintillator to tag cosmic ray particles passing through the shielding.

Each time a light pulse above 200 keV occurs in any cell or each time a cosmic ray counter gives a signal, the whole detector is digitized: PMT outputs are integrated with two 500 ns gates, the latter starting 25 ns after the beginning of the pulse for calculation of the $R_{PSD}$ value (Eq. (5)). The outputs of 5 integrators (total left, total

right and delayed charges as well as total and delayed charges in a smaller dynamic range optimized to the neutron capture (reaction (4)) are digitized using 8-bit 15 MHz FADC's clocked only once and the results of the conversions are stored in memory. The total dead-time is less than 2 $\mu$s. For economic reasons, distant elementary cells are grouped by 5 at the input of the integrators. However, each cell signal is also individually digitized using 6-bit 100 MHz FADC's with pseudo-log response for refined PSD and precise timing analyses. Pulses of the cosmic ray counters are integrated using standard ADC's [8]. Informations on the latest occurences (8 for integrators, 4 for 100 MHz FADC's, 16 for pattern and time units) are kept in memory and available at any time. For each occurence the time is read and stored from a 32 bit 2 MHz clock allowing the calculation of the time difference between two occurences. This electronics allows to check also the absence of particles correlated with a neutrino candidate event within several ms. Details of the performances of this electronics have been given elsewhere [8,11].

## 4. The trigger

The decision to record an event is taken with the help of a fast access programmable memory whenever the following conditions are satisfied:

- –occurrence of a neutron candidate: the $R_{PSD}$ value and the capture energy ($E_c$) are in the correct window. No other cell should fire at the same time and no cosmic ray counter should give a signal within 0.5 $\mu$s;
- –a positron candidate (a light pulse exceeding 200 keV energy) preceeds the neutron candidate by at most 100 $\mu$s;
- –the neutron and positron candidates are in the same or adjacent cells (proximity criterion).

The information from the cosmic ray counters was also used for off-line data reduction purposes and to monitor the stability of the neutron detection efficiency via the cosmic ray induced neutrons.

A special trigger to study accidentals was performed by requesting the above conditions with the neutron candidate preceeding the positron candidate.

The overall trigger rate was around 3 counts/s for one module. The overall trigger inefficiency (mainly due to accidental pulses occuring between the neutron and positron candidate) was close to $\approx 3\%$ at 15 m and to $\approx 6\%$ at 40 m and was corrected for in the data analysis.

Finally, let us mention here that the energy window used in the "neutron" definition was made wide enough to fully accept events corresponding to the Bismuth decay chain:

$$^{214}\mathrm{Bi} \rightarrow ^{214}\mathrm{Po} + \beta\ (3.27\,\mathrm{MeV}) \tag{6}$$

$$^{214}\mathrm{Po} \rightarrow ^{210}\mathrm{Pb} + \alpha\ (7.8\,\mathrm{MeV}\ \text{or}\ 820\,\mathrm{keV}\ e^{-}\ \text{equivalent}) \tag{7}$$

As the $^{214}$Po lifetime is 236 $\mu$s and the $\alpha$ signal is similar in energy and pulse shape to a neutron capture, a small part of this reaction contaminated the neutrino signal (see

Section 7). Radon outgasing from the detector materials was possibly at the origin of these events. We found that this rate was quite stable with time.

## 5. Calibration and monitoring

### 5.1. Reactor control.

- Thermal power values measured with an accuracy of 0.6% [12] on the three steam generators of the four reactors were provided by the reactor control group every 10 minutes. For the two nearest reactors less precise additional information was obtained from external neutron flux detectors which permitted to interpolate the precise thermal power values in case direct measurements were not available.
- An internal neutron flux distribution along the reactor axis with a bin size of 0.8 cm was provided each month. These measurements were used to simulate the vertical position of the reactor fission barycenter. Typically, this position did not vary by more than 6 cm during an annual fuel cycle.
- Cumulative burn-up values were provided each day and were used to simulate the variation of the composition of the four main fuel elements producing the anti-neutrinos in the reactor.

### 5.2. Gamma calibration and survey.

Each cell was calibrated every month using an Am–Be source emitting neutrons and 4.4 MeV gammas.

A dedicated anti-multi-Compton trigger helped to enhance the Compton edge at 4.2 MeV from which we deduced our energy scale and the electron (positron) $R_{PSD}$ value at this energy. The energy calibration constant was obtained using a detailed Monte Carlo program (see below) which reproduced well the measured shape of the Compton edge (see Fig. 3).

We calculated the overall uncertainty on the energy scale to be 0.034 MeV at 4.2 MeV. Our energy resolution at 4.2 MeV is 6% which was obtained from the upper half width of the Compton peak. A separate measurement with different gamma sources allowed us to verify the linearity of the whole opto-electronic chain [8] (see Fig. 4).

The overall gains of the opto-electronic chains were measured every day with the help of a monitored nitrogen spark-gap light pulser. The light pulses were brought simultaneously through optical fibers to the 98 cells and to several reference PMT's and photodiodes [13]. This procedure permits interpolation of the monthly calibrations and thereby follow up and correct for any variation in the transparency of the liquid or in the PMT gains. Typical day-to-day gain variations are shown in Fig. 5. Scintillator temperatures, low and high voltage values were recorded every 10 minutes.

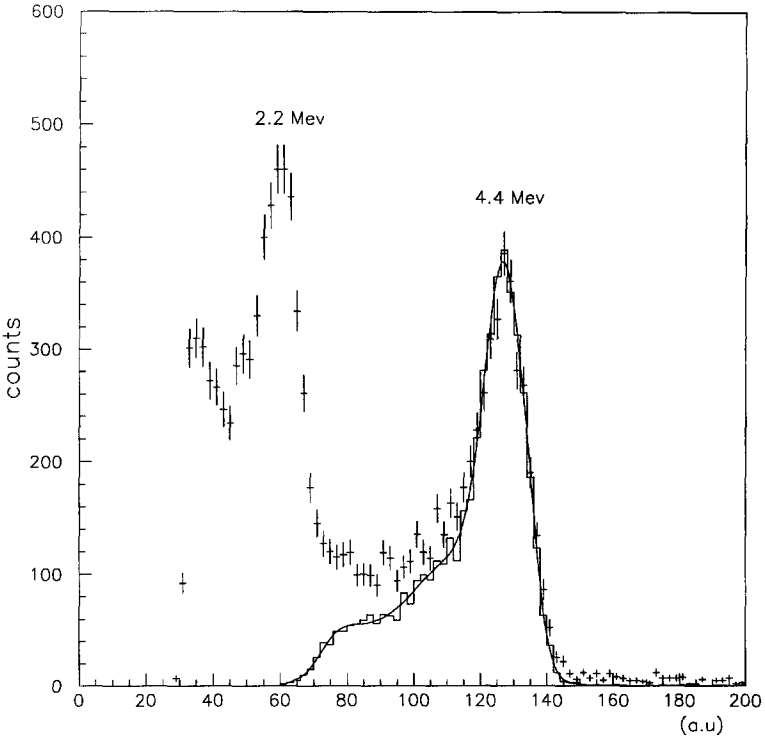


Fig. 3. The Compton edge of the 4.4 MeV photon obtained with an Am–Be source. The solid line is the Monte Carlo simulation (including the threshold effect of the calibration run). The peak near 2 MeV corresponds to gammas from the capture of neutrons in hydrogen not included in the simulation.

### 5.3. *Neutron calibration.*

By triggering on recoil protons we tag neutrons emitted by the Am–Be source to determine all parameters of the neutron capture by $^6$Li nuclei: the position and width of the capture energy peak, their variation along the longitudinal cell axis ($z$), as well as the PSD peak position and its width. Typical $R_{\mathrm{PSD}}$ and energy distributions of the neutron capture are depicted in Fig. 6.

Gamma, neutron and light-pulse calibrations were carried out using automated procedures, including source displacements. Successive determinations of the relevant parameters of each cell (positions of the 4.2 MeV backward Compton peak and of the neutron capture peak, $R_{\mathrm{PSD}}$ mean values and widths for electrons and captures, PMT gains) showed a reproducibility to better than 1% [8].

Fig. 7 shows the rate of muon induced neutrons tagged by cosmic ray counters and the number of photoelectrons as a function of time in module 1. One can see that despite the deterioration of the liquid with time the calibration ensured that the neutron detection efficiency remained stable.

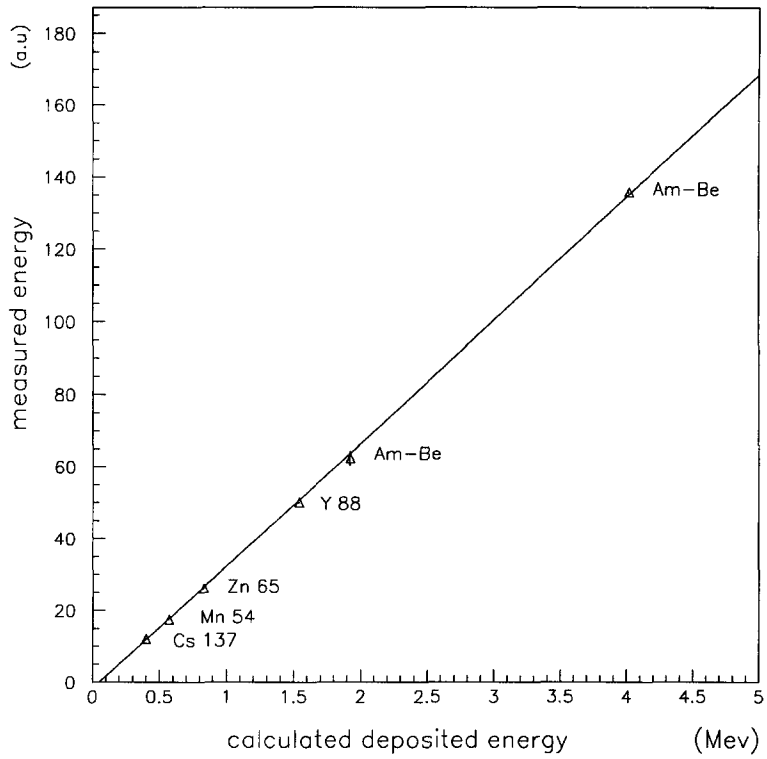


Fig. 4. The total charge measured at the end of the opto-electronic chain as a function of the deposited energy calculated by Monte Carlo for different gamma sources. The error bars are smaller than the symbols except at the 2 MeV peak which corresponds to the neutron capture in hydrogen. The linearity of the detector is clearly demonstrated.

## 6. Off-line data reduction

Triggers are rejected if a cosmic ray counter gave a signal in the preceding 100$\mu$s. This cut removes most of the cosmic ray induced background and gives 1.7% and 5.5% deadtime for the detection positions at 15 and 40 meters, respectively.

For each pulse, the longitudinal location ($z$) in the cell is determined by comparing the charges detected by the PMT's at both ends of the cell, and was used to correct the measured energy value.

Using results of neutron calibrations, an elliptical cut at 2.2 sigmas in the ($E_c$–$R_{PSD}^{neutron}$) plane is applied to neutron candidates.

The positron cell is defined as the one where the highest energy is deposited in case several cells were fired adjacent to the neutron cell. The positron energy ($E_{e^+}$), is required to be between 1 and 6 MeV with no simultaneous energy deposit ($E_{ext}$) bigger than 1.5 MeV outside the positron cell. The 1.0 MeV threshold of the positron is used to reduce the accidental background and to avoid confusion between the positron

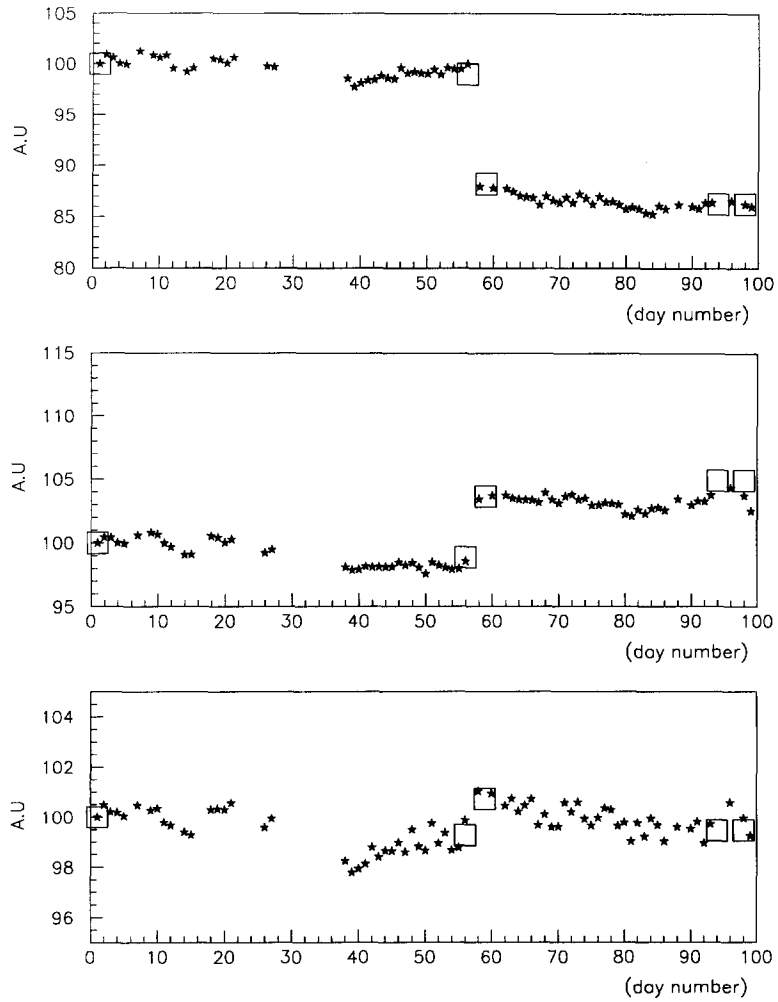


Fig. 5. Typical day-to-day gain variations of three channels measured with the help of a monitored nitrogen spark-gap light-pulser. The jumps correspond to reajustments of the high voltage setting point. The results of the calibration with the Am–Be source are shown by the squares.

cell and any other one in which the 511 keV annihilation gamma rays would have been converted.

A $3\sigma$ cut is performed on the $R^{e^+}_{\mathrm{PSD}}$ of the positron candidate to reject recoil protons induced by fast neutrons whose thermalization and capture would fake neutrino events.

Finally, refined proximity criteria between the positron and the neutron candidates are applied:

- the positron candidate should precede the neutron candidate by at most 60 $\mu$s;
- the two candidates should be either in the same cell or in adjacent cells having a common face;

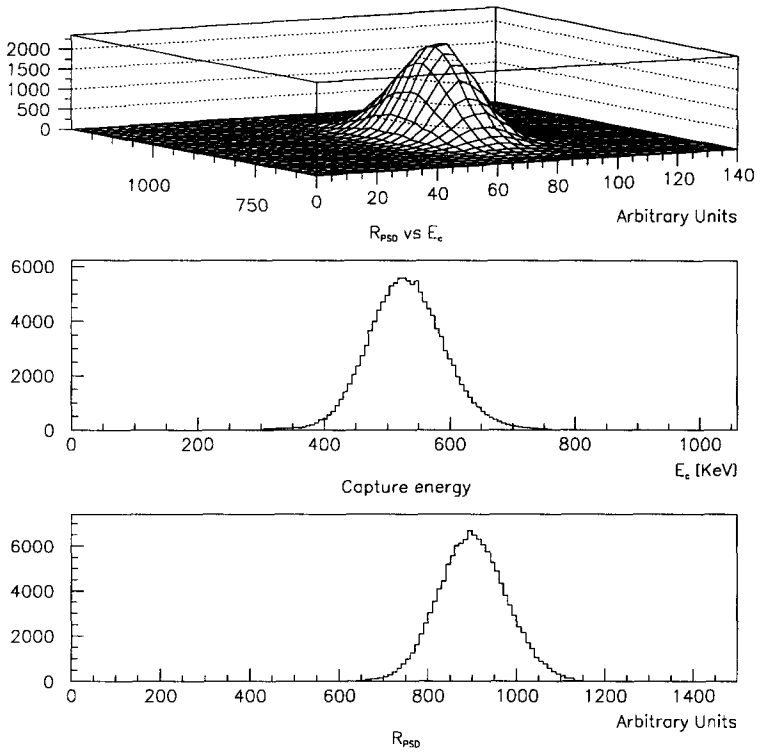


Fig. 6. $R_{PSD}$ and energy distribution of the neutron capture obtained during calibration run by an Am–Be source.

–their separation in $z$ should be smaller than 35 cm.

These selection criteria have been applied in two steps: in the event filtering phase where they were somewhat relaxed and in the final event selection phase. As an example we give in Table 1 module 1 rates obtained in the two data reduction phases.

The same analysis is performed on accidental triggers in order to subtract them from the neutrino signal.

The statistics accumulated in various conditions are summarized in Table 2.

## 7. Background subtraction and corrections

Earlier measurements have shown [4] that the reactor-correlated background is negligible at our measurement positions. Therefore in the following we will deal only with the background which is uncorrelated to the reactor and thus in principle can be subtracted by measurements carried out when the reactor is stopped.

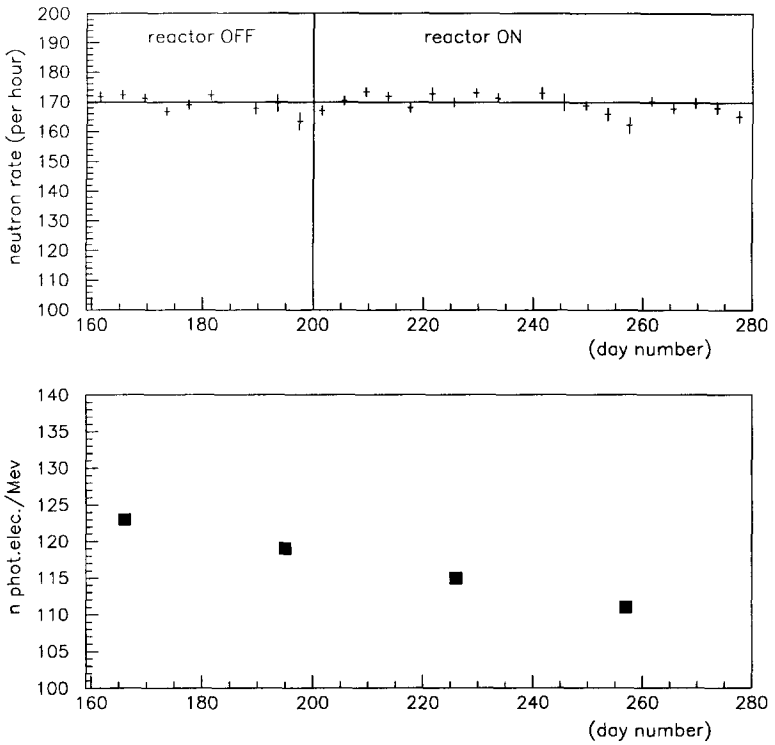


Fig. 7. The time evolution of the rate of the cosmic neutrons (upper part) and that of the number of the photoelectrons (lower part) in module 1.

Table 1
Event rates obtained for module 1 applying different selection criteria.

| Selection | Rate [Hz] |
|---|---|
| On-line trigger | $\sim 3$ |
| Off-line event filter:<br>Veto against cosmic<br>$E_{e^+} > 400\,\text{keV}$<br>($R_{\text{PSD}}^{\text{neutron}}$ vs. $E_c$) $3\sigma$ cut<br>Spatial coincidence | 0.14 |
| Final selection:<br>$1 < E_{e^+} < 6\,\text{MeV}$<br>$E_{\text{ext}} < 1.5\,\text{MeV}$<br>($R_{\text{PSD}}^{\text{neutron}}$ vs. $E_c$) $2.2\sigma$ cut<br>$R_{\text{PSD}}^{e^+}$ $3\sigma$ cut<br>time coincidence ($2.5 < \tau_{n-e^+} < 60\ \mu$)s | 0.017 |

Table 2
Event statistics.

| | 15m | | 40m | | | | 95m | |
|---|---|---|---|---|---|---|---|---|
| | mod 1 | | mod 2 | | mod 3 | | mod 1 | |
| Reactor status [a] | On | Off | On | Off | On | Off | On | Off |
| $\nu$ candidate events | 92519 | 3746 | 14624 | 6840 | 32430 | 4785 | 1865 | 223 |
| Accidental events | 1640 | 1166 | 3620 | 4527 | 5451 | 2908 | 464 | 98 |
| Measurement time (h) | 1734 | 1436 | 1496 | 1837 | 3094 | 1725 | 660 | 135 |
| Mean power [a] (MW) | 2699 | | 2524 | | 2611 | | 2656 | |

[a] Nearest reactor except for 95 m where it refers to the second nearest reactor, the nearest one being off.

Table 3
Accidental background rates in $h^{-1}$.

| | On | Off |
|---|---|---|
| module 1 | $1.17 \pm 0.03$ | $1.07 \pm 0.03$ |
| module 2 | $2.68 \pm 0.04$ | $2.61 \pm 0.04$ |
| module 3 | $1.92 \pm 0.02$ | $1.78 \pm 0.03$ |

### 7.1. *Accidental background.*

The accidental background at the first order is equal to the accidental trigger events passing through the data reduction cuts.

The accidental background rates for the three modules and in the reactor-on and off periods are summarized in Table 3.

Energy spectra and time distributions between positron and neutron candidates for the accidental component of the background are shown for the module 1 in Fig. 8a and Fig. 9.

### 7.2. *Correlated background.*

Data taken during reactor-off periods give us the rate of the correlated component of the background once the accidental background is subtracted. This rate is equal to $2.22 \pm 0.06$ events/h in module 1, $1.32 \pm 0.06$ events/h in module 2 and $1.15 \pm 0.05$ events/h in module 3. In Fig. 8a and in Fig.9 we have inserted the energy spectra and the time distribution of the residual correlated background for module 1. For modules 2 and 3 the shapes of these distributions are similar.

It is possible to identify the origin of part of the correlated background as being the "Bismuth" events by applying all the off-line selection criteria (see Table 1) except the

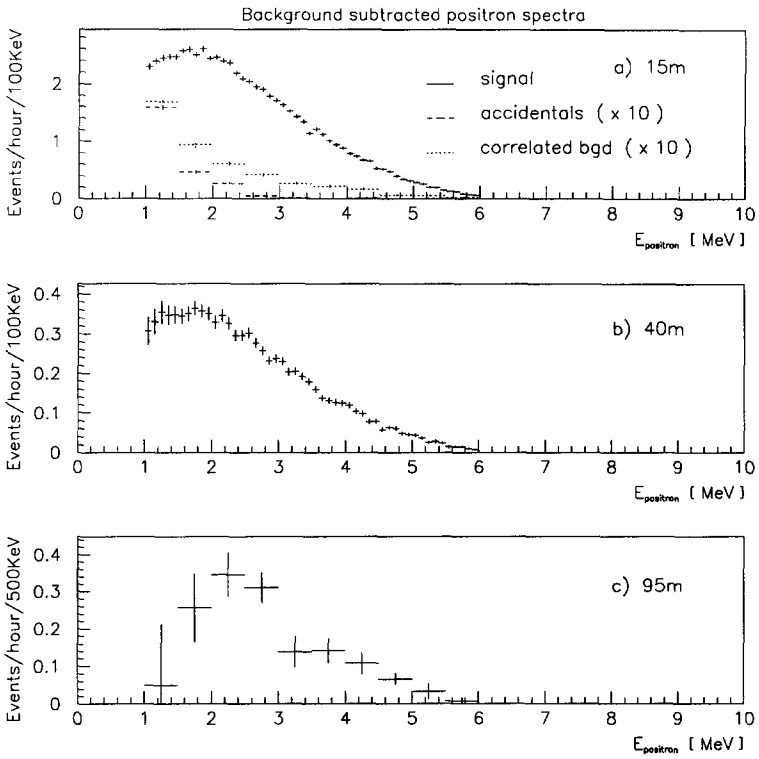


Fig. 8. Normalized positron spectra obtained (a) at 15 m, (b) at 40 m and (c) at 95 m distances the background being subtracted. The various background components at 15 meter are also shown in (a).

Table 4
Average "Bismuth-event" background rates in $h^{-1}$.

| | On | Off |
|---|---|---|
| module 1 | $0.52 \pm 0.03$ | $0.52 \pm 0.06$ |
| module 2 | $0.19 \pm 0.07$ | $0.24 \pm 0.04$ |
| module 3 | $0.12 \pm 0.05$ | $0.05 \pm 0.03$ |

full $R_{PSD}$–$E_c$ elliptical cut which is replaced by a simple $R_{PSD}$ cut at $\pm 2.2$ sigma (no energy selection at the high end). In the upper part of Fig. 10 which shows the energy spectrum of the neutron candidates in module 1 satisfying these conditions, the $\alpha$-peak at 820 keV of reaction (7) is clearly seen.

The rate of this part of the background has been estimated by the data taken in reactor-on and off periods separately. We made use of the fact that the $^{214}$Po lifetime (236 $\mu$s) is much longer than the neutron capture time (30 $\mu$s) in reactions (2), (4). Table 4 shows the average rate of that part of the "Bismuth events" in the three detection modules which satisfies the data selection criteria and thus contaminates the neutrino events. As can be seen (cf. also Fig. 10) the background event rates are practically

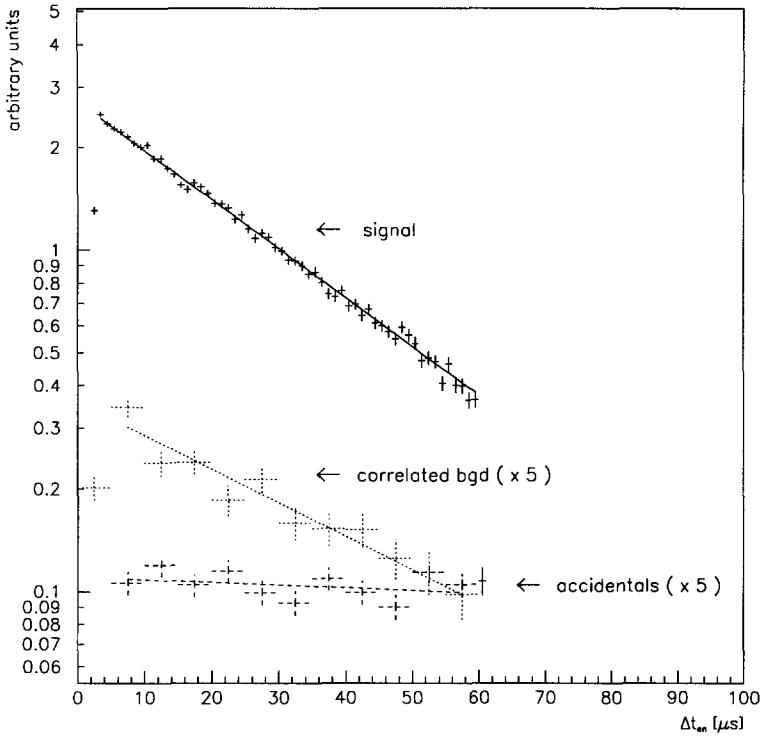


Fig. 9. The observed time distribution is in agreement with the pure random coincidences between heavy and light particles expected from their measured single rates. The accidental rate is higher in module 2 and 3 due to the different contamination of the liquid by $\alpha$ emitters as explained earlier.

the same in the reactor-on and off periods, therefore a simple subtraction On–Off can eliminate this background.

The remaining part of the correlated background (apart from the genuine neutrinos produced by the faraway reactors) consists mainly of fast neutrons induced by cosmic rays. This is illustrated for module 1 in Fig. 11 where the positron $R_{PSD}$ of the data is shown when all selection criteria are applied except the positron $R_{PSD}$ cut.

The bump at high $R_{PSD}$ values is due to protons recoiling from fast neutrons in the neutron thermalization process. Part of these protons survive the positron $R_{PSD}$ cut. Table 5 shows the observed rates of this type of background events for the three modules. As can be seen in Table 5 and in Fig. 11 the magnitude of the peak at high $R_{PSD}$ is the same for reactor on and off periods thus this type of background is eliminated by subtracting the correlated background measured in the reactor off period from that of the reactor-on period.

In Table 6 we compile at the 15 meter position the observed rates due to the different background components in reactor-off periods. As one can see, the sum of the average correlated background rates determined individually in the reactor-off periods is in good agreement with the average rate of the observed correlated events in the same period.

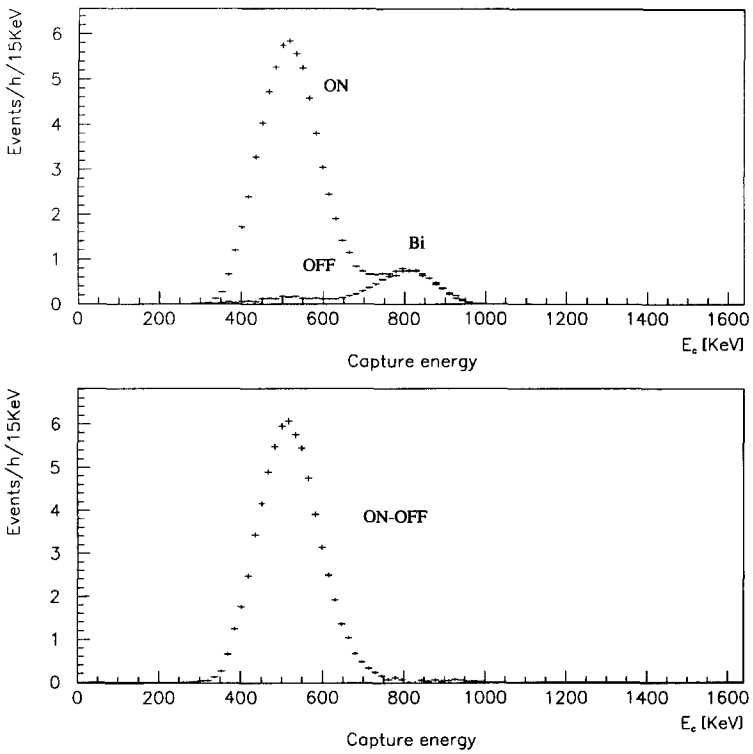


Fig. 10. The ($e^-$-equivalent) neutron capture energy spectrum (in events/h/15 keV) of the events passing all selection criteria except the neutron energy cut in module 1 for reactor-on and reactor-off periods (upper part) and the difference of the reactor-on and reactor-off periods (lower part).

Table 5
Background rates in $h^{-1}$ from cosmic ray induced fast neutrons.

| | On | Off |
|---|---|---|
| module 1 | $1.2 \pm 0.4$ | $0.7 \pm 0.2$ |
| module 2 | $0.6 \pm 0.2$ | $0.6 \pm 0.2$ |
| module 3 | $0.7 \pm 0.2$ | $0.5 \pm 0.2$ |

Table 6
Average background rates in $h^{-1}$ in reactor-off periods at 15 m.

| | | |
|---|---|---|
| Accidentals | | $1.07 \pm 0.03$ |
| Bismuth events | $0.52 \pm 0.06$ | |
| Fast neutrons | $0.70 \pm 0.20$ | |
| $\nu$'s from far reactors | $0.89 \pm 0.01$ | |
| Sum of components | $2.11 \pm 0.21$ | |
| Total correlated events | | $2.22 \pm 0.06$ |
| Total background | | $3.29 \pm 0.07$ |

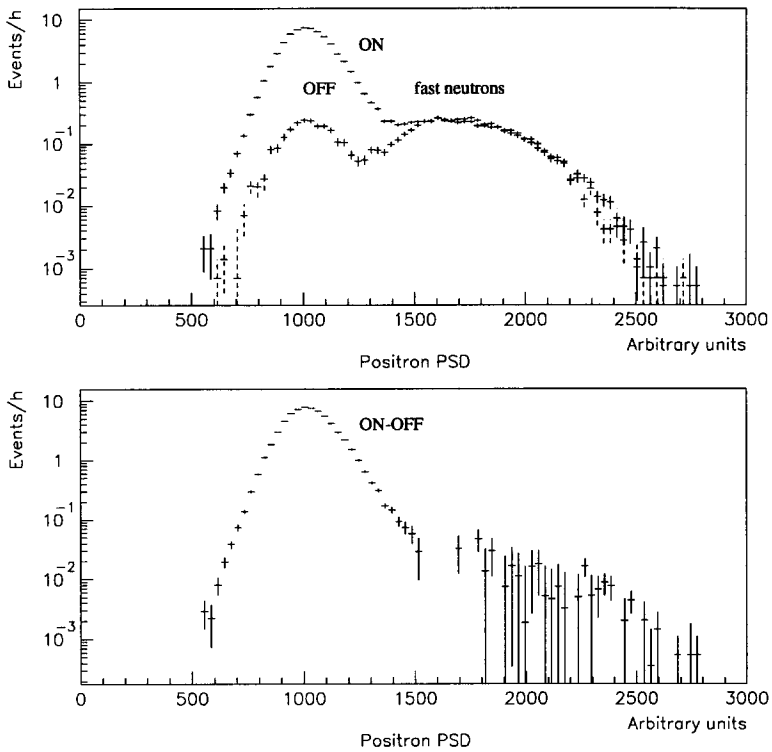


Fig. 11. The positron $R_{PSD}$ distribution of the events passing all selection criteria except the positron $R_{PSD}$-cut in module 1 for reactor-on and reactor-off periods (upper part) and the difference of the reactor-on and reactor-off periods (lower part).

The observed event rates are corrected for the deadtime of the detector modules, for losses due to electronics or HV power failures in some detection channels. The event rate due to anti-neutrino interactions (signal) is obtained by subtracting first the accidental background from the data separately in the reactor-on and off periods since we observe slight differences in these rates with time. Next, the remaining events from the reactor-off period are subtracted from the remaining reactor-on events. The actual signal event rates, the total background rates and the signal-to-background ratios above 1 MeV are summarized in Table 7 for 15, 40 and 95 meters [14], respectively. All errors indicated are statistical only.

The signal event rates are finally corrected for the expected number of neutrino events from faraway reactors and normalized at each detection position for the same target mass (corresponding to the volume of one full detector module) and to a nominal 2800 MW thermal power of the reactor. The normalized positron spectra are shown in Fig. 8 for 15 m, 40 m and 95 m distances, respectively.

Table 7
Average signal event and total background rates in $h^{-1}$ at the three distances.

| | 15 m | 40 m [a] | 95 m |
|---|---|---|---|
| Signal event rate | $62.62 \pm 0.23$ | $15.39 \pm 0.17$ | $1.38 \pm 0.20$ |
| Total background rate (without $\nu$'s from far reactors) | $2.50 \pm 0.07$ | $6.94 \pm 0.09$ | $1.96 \pm 0.18$ |
| Signal/background | 25.0 | 2.2 | 0.7 |

[a] For the two modules.

## 8. Data analysis and results

In order to test the oscillation hypothesis we used two methods:

(i) in the first one we compared the experimentally observed *ratios* of positron spectra at two different distances to the ratios predicted by Monte Carlo. It has the advantage that uncertainties on the absolute detection efficiencies and on the neutrino flux and spectrum do not enter at first order.

(ii) In the second method we compared the *normalized* positron energy spectra measured at different distances with those expected from the Monte Carlo calculations taking into account the absolute detection efficiencies, neutrino flux and spectrum. This method has the advantage to include information also on the neutrino source in the test of the oscillation hypothesis. Furthermore it is a test that the reactor spectrum used was adequate in our sensitive energy region.

For this analysis we have carried out a detailed simulation of the signal events including:

- -simulation of the neutrino flux and spectrum for each day of the data taking;
- -simulation of the neutrino interaction in hydrogen (reaction (2)) together with the capture of the produced neutron (reaction (4)) and the detection of the products of the capture;
- -simulation of the detection of the positron in reaction (2) and the measurement of its energy.

The simulated signal events were submitted to the same cuts as applied for the data. The different background components were not simulated since they were directly subtracted from the data (see previous section).

### *8.1. Monte Carlo simulation.*

#### *8.1.1. Neutrino spectrum.*

The energy spectrum of the neutrinos incident on the detector is simulated [15] using the measured $\beta$ spectra of the main fission products ($^{235}$U, $^{239}$Pu, and $^{241}$Pu) by the authors of Ref. [16] and calculated (for $^{238}$U) in Ref. [17]. The time dependence of the composition of the fuel elements and the horizontal distribution of the neutrinos produced inside the reactor core are computed from the exact burn-up values of the combustible arrays delivered at the beginning and at the end of each operation period by the reactor control group and interpolated daily from the thermal power data. Their vertical distribution is obtained using corresponding measurements by the reactor control

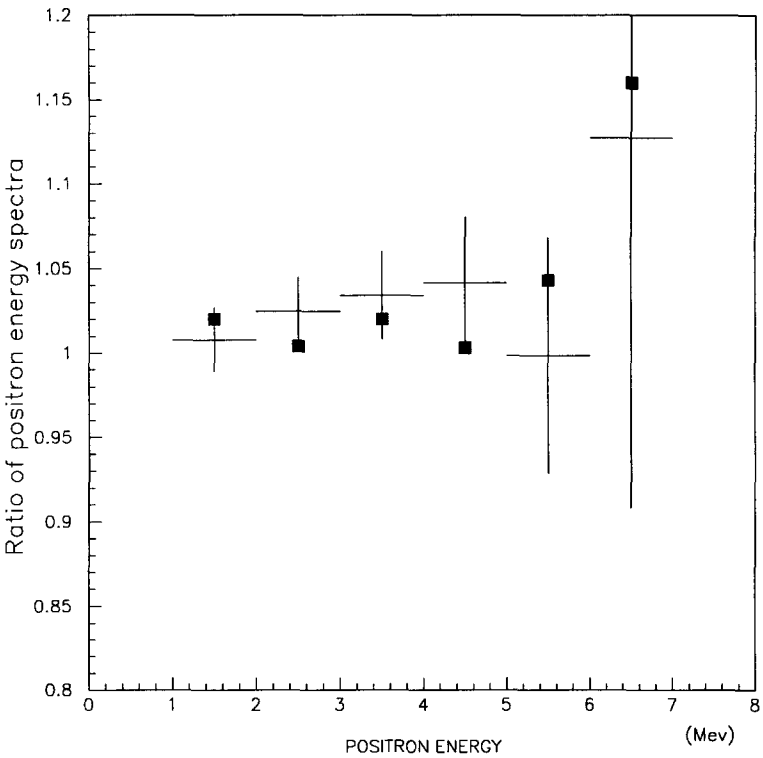


Fig. 12. The ratio of the positron spectra measured at a given time and 100 days later (at 15 m). The squares represent the Monte Carlo calculation. The error bars of the Monte Carlo are not shown for clarity, they are much smaller than those of the data.

group as mentioned in Section 5 above. The neutrino spectrum has a systematic error of 2.4% due to the measurement error and the uncertainties of the applied method in Ref. [16] which gradually increases with energy reaching $\sim$ 5–7% around 8 MeV.

We have compared the simulated and measured time variation of the positron spectrum (both in intensity and shape) due to burn-up. Fig. 12 shows the ratio of the positron spectra measured at a given time and 100 days later at 15 m and at full reactor power. As can be seen the observed and simulated ratios agree within errors and the simulation reproduces correctly the evolution of the neutrino spectrum with time.

*8.1.2. Neutrino interaction and neutron capture.*

In simulating reaction (2) we included radiative corrections [18] and neutron recoil.

A special program was written [19] and linked to GEANT [20] which simulates the neutron thermalization and capture in $^6$Li in the $10^{-3}$–$10^7$ eV energy range by following the neutron slowing down process using BNL cross sections [21] and including the appropriate Maxwell distribution of the thermal neutrons and the binding of the proton to its molecule. We have verified the validity of this simulation on data of previous measurements [3,26] and in special calibration runs where the absolute detection efficiency

Table 8
Decomposition of the neutron detection efficiency.

| | |
|---|---|
| Total capture probability | 0.898 |
| Capture on the $^6$Li component | 0.885 |
| Volume seen by PMT's | 0.912 |
| Cut on capture time | |
| $2.5 < \tau_{n-e^+} < 60$ $\mu$s | 0.756 |
| Spatial proximity criterion | 0.892 |
| Overall neutron detection efficiency | 0.489 |

of fast neutrons was measured [8]. The obtained detection efficiency agreed within 1.3% with that of the simulation. The overall neutron detection efficiency together with its decomposition is given in Table 8.

*8.1.3. Detection of the positron and Compton scattering.*

We have simulated in detail the response of the detector for Compton scattering. The simulation also contains the detection of the positron including its energy deposition inside the detector material (the slowing down of the positron, the two-gamma positron annihilation in flight and at rest) [20,22] and the light collection process together with the occasional saturation of the electronics [23]. For the Compton scattering part, used to obtain the positron energy calibration constant, two independent programs have been written which agreed within 0.3%. The programs have been partly tuned or checked on calibration data, as well as on dedicated Compton backward scattering measurements with collimated photons which enabled us to determine experimentally the light collection along the cell axis (see Fig. 13).

The simulation showed that the systematic uncertainty in the positron energy calibration is 0.034 MeV at 4.2 MeV. This error induces a systematic error in the positron energy spectrum which increases with the positron energy and is correlated from one energy bin to another. This latter is further increased owing to our finite precision in the way we could simulate the positron trajectory and its back scattering in the wall of the optical tunnel as well as our limited knowledge in the quantity of the inactive material of this latter. It was found by the simulation that such a systematic error can be taken into account by multiplying the positron spectrum by a linear factor $(a+b\cdot(E_{e^+}-E_0))$ where $b$ is centered around zero with an uncertainty of $\pm 0.014\,\mathrm{MeV}^{-1}$ and $E_0$ is 1 MeV.

The correctness of the simulation can be illustrated by comparing some typical data distributions with those obtained by the Monte Carlo. As an example Fig. 9 shows the time difference distribution between the positron and the neutron capture in module 1. An exponential fit gives a mean capture time of $29.71 \pm 0.21$ $\mu$s for the data, whereas the Monte-Carlo value is $30.19 \pm 0.16$ $\mu$s (the errors are statistical only). Fig. 14 shows the horizontal and vertical distribution of the anti-neutrino events at 15 m. The detector edges are underpopulated due to neutron leakage. In module 1 the decrease between top and bottom is due to the variation of the solid angle upon which the reactor core is seen from the different cells. This feature is well described by the Monte Carlo simulation.

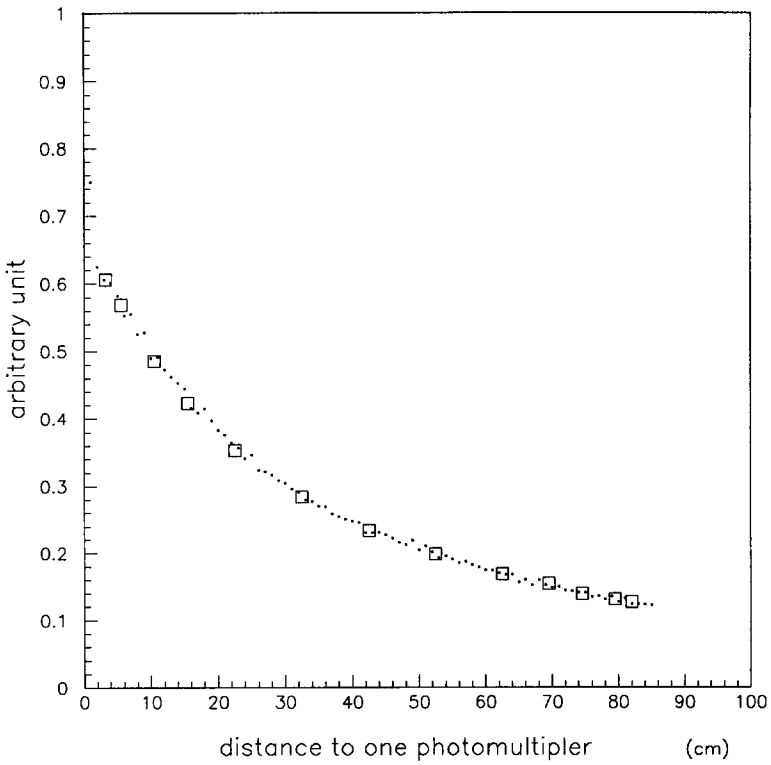


Fig. 13. The light collected by one of the two PMT's as a function of the $z$ position of the positron. Squares: data, dotted line: Monte Carlo.

*8.1.4. Normalization errors.*

We distinguish two cases. In the first one we list the quantities and their errors which enter when comparing the *absolute* rates (spectra) between data and Monte Carlo. In the second one only those quantities and errors are mentioned which play a rôle when comparing data and Monte Carlo *relative* rates (spectra) from one position to another.

*Absolute normalization*:

- Error on the neutrino flux: $\pm$ 2.8% (the spectrum in Ref. [16] and reactor control);
- Cross section of reaction (2) which depends on the neutron lifetime [25] whose latest value (889 $\pm$ 2) s is taken from Ref. [24];
- The distances between the center of the nearest reactor core and that of the detectors have been measured to an accuracy of $\pm$2 cm. To this we add an error of $\pm$3 cm on the determination of the barycenter of the active core with the help of the internal neutron flux measurement. This introduces a negligible error on the solid angle upon which the detectors are seen at 40 m and an error of $\pm$ 0.5% at 15 m;

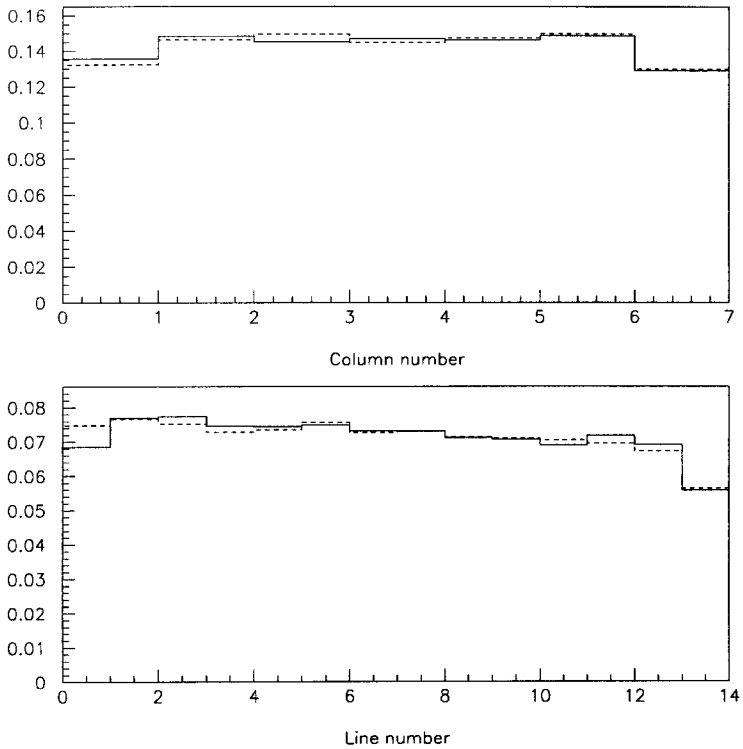


Fig. 14. Horizontal (column) and vertical (line) distribution of the neutrino events at 15 m (solid line: data, dotted line: Monte Carlo).

-Error on the volume of the active part of the target: $1.5 \times 1.25\% = 1.9\%$, where the 1.25% is due to the uncertainties in the geometrical shape of the light tunnel and the factor 1.5, determined by Monte Carlo, takes into account that the error should be applied both for the neutrons and positrons;
-Error on the overall neutron detection efficiency (not including that due to volume) $\pm$ 3.2%;
-Error on the overall positron detection efficiency (not including that due to volume) $\pm$ 0.9%;
-Error on the neutron–positron space-time correlation $\pm$ 1%.

*Relative normalization*:
-Error on the solid angle: $\pm$ 0.5%;
-Error on the the volume of the active part of the target: $\pm$ 0.6%;
-Error on the neutron efficiency, estimated from the survey of the Bi-event and cosmic ray induced fast neutron rates: $\pm$ 1.5%;
-Error on the positron detection efficiency: $\pm$ 0.9%.

Table 9
Errors on the normalization.

| | Relative error in % | |
|---|---|---|
| | Abs. norm. | Rel. norm. |
| Neutrino flux | 2.8 | |
| $\nu p$ Cross Section | 0.2 | |
| Solid angle | 0.5 | 0.5 |
| Number of protons | 1.9 | 0.6 |
| Neutron detection eff. | 3.2 | 1.5 |
| Positron detection eff. | 0.9 | 0.9 |
| Neutron-positron corr. | 1.0 | |
| Total | 5.0 | 2.0 |

All these errors are related to 1 standard deviation (68% of confidence level). They are listed also in Table 9.

*8.1.5. Ratios of energy spectra.*

Fig. 15 shows the ratios of the positron spectra at 40/15 m and at 95/15 m. For the ratio 40/15 m we show separately the part of the data taken simultaneously and therefore totally independent of the fuel evolution of the reactor.

The ratios exhibit no variation with the positron energy and their fitted values of $0.140 \pm 0.001$ and $0.025 \pm 0.001$ correspond well to $(15/40)^2$ and $(15/95)^2$, the ratios of the solid angles upon which the detectors are seen from the center of the reactor cores. Since the response functions are the same at the two measurement positions the observed ratios are compatible with *no oscillation* of the produced anti-neutrinos.

In order to quantify this statement we consider the following $\chi^2$:

$$\chi^2_{P1,P2} = \sum_{i=1}^{N} \frac{\left(aR^{\text{the}}_{P1,P2,i}(\delta m^2, \sin^2 2\theta) - R^{\text{obs}}_{P1,P2,i}\right)^2}{\sigma_i^2} + \frac{(a-1)^2}{\sigma_a^2}. \tag{8}$$

Here $R^{\text{obs}}_{P1,P2,i}$ is the ratio of the number of signal events/$h$ in the $i$th positron energy bin of 200 keV width, measured at two different positions, $P1$ and $P2$, and normalized at each position to the same target mass (1 full module) and thermal power (2800 MW). $R^{\text{the}}_{P1,P2,i}(\delta m^2, \sin^2 2\theta)$ is the theoretically expected ratio calculated by Monte Carlo at a given point in the $\delta m^2$–$\sin^2 2\theta$ plane, $\sigma_i^2$ is the combined statistical error of $R^{\text{the}}_{P1,P2,i}$ and $R^{\text{obs}}_{P1,P2,i}$. $a$ and $\sigma_a$ are the *relative* normalization at the two different positions and its error. This latter is taken to be the same for all ratios and its value is given in Table 9 as the total error on the relative normalization.

We calculate the minimum of this $\chi^2$ with respect to $a$ at a fixed value of $\delta m^2$ which we call $\chi^2_{R,P1,P2}(\delta m^2, \sin^2 2\theta)$. $\chi^2_{R,P1,P2}$ is thus a function of $\sin^2 2\theta$ only with a minimum for a given value of $\sin^2 2\theta_{\min}$. As $R^{\text{the}}_{P1,P2,i}(\delta m^2, \sin^2 2\theta)$ is approximately linear in $\sin^2 2\theta$ (cf. Eq. (1)) the difference

$$D(\sin^2 2\theta) = \chi^2_{R,P1,P2}(\sin^2 2\theta) - \chi^2_{R,P1,P2}(\sin^2 2\theta_{\min})$$

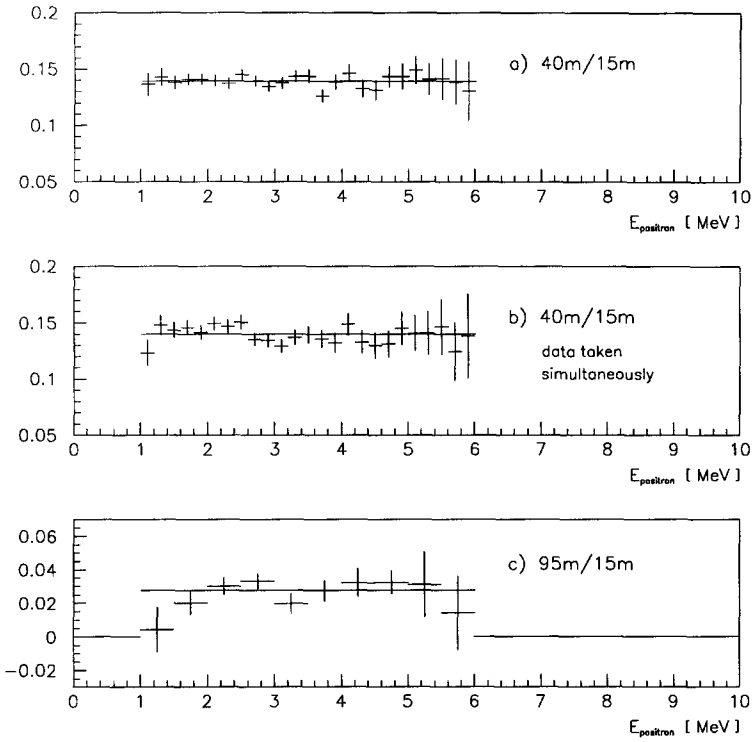


Fig. 15. The ratio of the positron energy spectra at 40/15 m (upper) and 95/15 m (lower part). Also shown for 40/15 m the part of the data taken simultaneously (middle part). The solid lines indicate the result of the fit to a constant line.

obeys a 1 degree-of-freedom $\chi^2$ law when $\delta m^2$ is at the true value. We use this property to evaluate an acceptance domain at 90% confidence level[3] for $\sin^2 2\theta$ following the procedure described in Ref. [24], when the physical region is bounded ($\sin^2 2\theta \geqslant 0$). Fig. 16 shows the exclusion contours obtained in this way separately for 40/15 and 95/15 meters, right to which the oscillation parameters are excluded at 90% confidence level. The $\chi^2$ values for the non-oscillation hypothesis and the minimum values of the $\chi^2$ in the $(\delta m^2, \sin^2 2\theta)$ plane are given in the first two rows of Table 11.

*8.1.6. Normalized energy spectra.*

Fig. 17 shows the ratios of the observed positron spectra to the ones predicted by our Monte Carlo calculation in the absence of oscillations at 15, 40 and 95 meters.

[3] The a priori more standard method, based on the *simultaneous* minimization of $\sin^2 2\theta$ and $\delta m^2$ is more intricate since the function to be fitted is not linear in $\delta m^2$. Thus the difference $D(\delta m^2, \sin^2 2\theta) = \chi^2_{R,P1,P2}(\delta m^2, \sin^2 2\theta) - \chi^2_{R,P1,P2}(\delta m^2_{\min}, \sin^2 2\theta_{\min})$ does not obey any known law and its distribution would have to be simulated numerically for each value of $(\delta m^2_{\text{true}}, \sin^2 2\theta_{\text{true}})$.

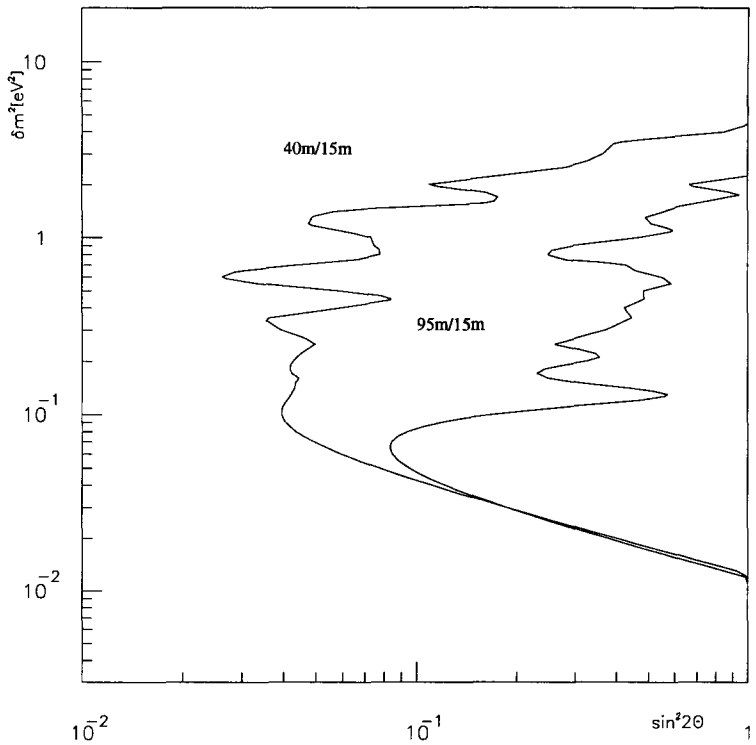


Fig. 16. 90% C.L. exclusion contours obtained from the ratios of the positron energy spectra measured at 40/15 and 95/15 meters.

All ratios are compatible with 1 in the energy region of 1 to 6 MeV, taking into account our estimated systematic error indicated by the corridor in the figure. This latter has the form of $1 \pm \sqrt{\sigma_{an}^2 + ((E_{e^+} - E_0)\sigma_b)^2}$, where $\sigma_{an}$ is the total error on the absolute normalization in Table 9. For $\sigma_b$ we have taken the conservative value of $0.02\,\mathrm{MeV}^{-1}$ which includes also the uncertainty of the global shape of the reactor neutrino spectrum.

The normalized energy spectra thus confirm our previous conclusion on the absence of oscillations and at the same time they underline the validity of the neutrino spectrum used in the simulation [16]. The obtained ratios of the measured integrated yields between 1 and 6 MeV with respect to the expected ones in the absence of oscillations are listed in Table 10. They all agree with 1 well within the quoted errors.

There are several sources of systematic errors, as already quoted before:

- an uncertainty of the measured spectrum of the emitted neutrinos by the reactor;
- an error in the positron energy scale;
- an error in the estimation of the quantity of the inactive material of the detector;
- an error in the simulation of the true positron trajectory, and
- an error in the correction for the saturation of the electronics due to anomalously high light pulses produced in the vicinity of the PMT's.

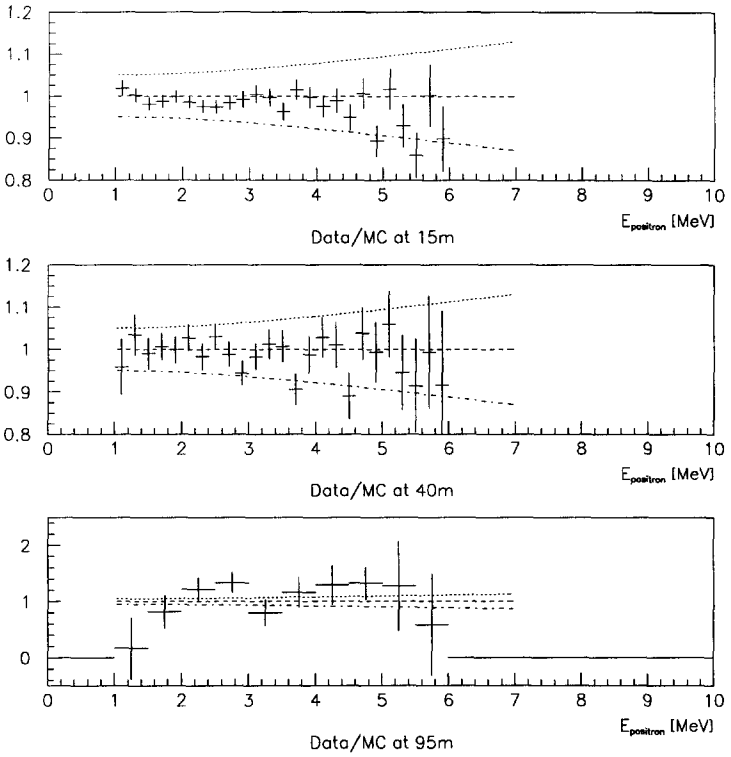


Fig. 17. The ratio of the observed and the predicted positron spectra in the absence of oscillations: at 15 meters (upper), at 40 meters (middle), and at 95 meters (lower part). The band corresponding to the estimated systematic error is also shown (see text).

Table 10
Ratios of the measured and calculated (without oscillations) integrated yields.

| Position | Ratio |
|---|---|
| 15 m | $0.988 \pm 0.004$ (stat) $\pm 0.05$ (syst) |
| 40 m | $0.994 \pm 0.010$ (stat) $\pm 0.05$ (syst) |
| 95 m | $0.915 \pm 0.132$ (stat) $\pm 0.05$ (syst) |

We have taken into account these systematic errors by a deformation of the positron spectrum with an ad hoc function depending on the positron energy. Since the effects are small we developed this function up to the linear term only. (As written above this is justified by our Monte Carlo simulation.) The parameters of this developement (with the exception of $E_0$ which we fix to a value of 1 MeV) are determined by minimizing the $\chi^2$ in the process of the determination of the exclusion contour. Using simultaneously the measurements at all the three distances and the spectrum of the emitted neutrinos we consider the following $\chi^2$:

Table 11
$\chi^2$ values.

| Distances | Minimum of $\chi^2$ at | | $\chi^2_{\min}$ | $\chi^2(0,0)$ | N.D.F. |
|---|---|---|---|---|---|
| | $\delta m^2$ | $\sin^2 2\theta$ | | | |
| 15/40 | 1.60 | 0.09 | 17.53 | 20.04 | 25 |
| 15/95 | 0.45 | 0.35 | 20.56 | 26.12 | 25 |
| $15 \oplus 40 \oplus 95$ | 1.70 | 0.05 | 47.53 | 50.15 | 60 |
| meters | 0.90 | 0.03 | 47.68 | | |

$$\chi^2 = \sum_{j=1}^{3} \left[ \sum_{i=1}^{N} \frac{\left((Aa_j + b(E_{e^+} - E_0))S_{j,i}^{\text{the}}(\delta m^2, \sin^2 2\theta) - S_{j,i}^{\text{obs}}\right)^2}{\sigma_{j,i}^2} + \frac{(a_j - 1)^2}{\sigma_{a_j}^2} \right] + \frac{(A-1)^2}{\sigma_A^2} + \frac{b^2}{\sigma_b^2}. \tag{9}$$

Here $S_{j,i}^{\text{obs}}$ is the number of the signal events/$h$ in the $i$th positron energy bin of 200 keV width, measured at position $j$ and normalized to the same target mass (1 full module) and thermal power (2800 MW). $S_{j,i}^{\text{the}}(\delta m^2, \sin^2 2\theta)$ is the corresponding number of events expected with oscillation parameters $\delta m^2, \sin^2 2\theta$ calculated by Monte Carlo. $\sigma_{j,i}$ is the error on the corresponding numerator. It is dominated by the statistical error of the data and includes also (i) the statistical error of the Monte Carlo simulation, (ii) the statistical error of the measured $\beta$-spectra [16] and (iii) the bin-to-bin systematic error of the procedure which gives the neutrino spectrum from the measured $\beta$-spectra [29]. $A$ is a common normalization factor for the three positions whereas the normalization factors $a_j$ ($j = 1,2,3$), vary independently from position to position. As mentioned already earlier, the bias $b$ is the parameter which together with $A$, $E_0$ and with the $a_j$'s represents the large scale deformation of the positron spectrum due to systematic effects. For all $\sigma_{a_j}$ we have taken $1/\sqrt{2}$ times the total relative normalization error listed in Table 9. On the other hand, $\sigma_A = (\sigma_{\text{an}}^2 - \sigma_{a_j}^2)^{1/2}$, where $\sigma_{\text{an}}$ is the total error on the absolute normalization in Table 9, as mentioned before.

The minimization procedure is essentially the same as explained in the case of the ratios. At fixed $\delta m^2$ we calculate the minimum of the above $\chi^2$ for all other parameters ($A$, $a_j$, ($j = 1,2,3$), $b$) except for $\sin^2 2\theta$ and we evaluate again an acceptance domain at 90% confidence level for $\sin^2 2\theta$ following the procedure mentioned above. This gives us an overall exclusion contour when all available experimental information is used. The result is shown in Fig. 18 together with the largest exclusion contour obtained in earlier reactor experiments [26,27], and also with the region for a possible $\nu_e - \nu_\mu$ oscillation put forward by the KAMIOKANDE collaboration [28]. The minimum value of the $\chi^2$ in the $(\delta m^2, \sin^2 2\theta)$ plane and the $\chi^2$ value for the non-oscillation hypothesis are given in Table 11 (in fact we obtain two minima of $\chi^2$ values very close to each other). Again, the obtained $\chi^2$ values support the hypothesis of non-oscillation and at the same time show the adequacy of the used reactor spectrum.

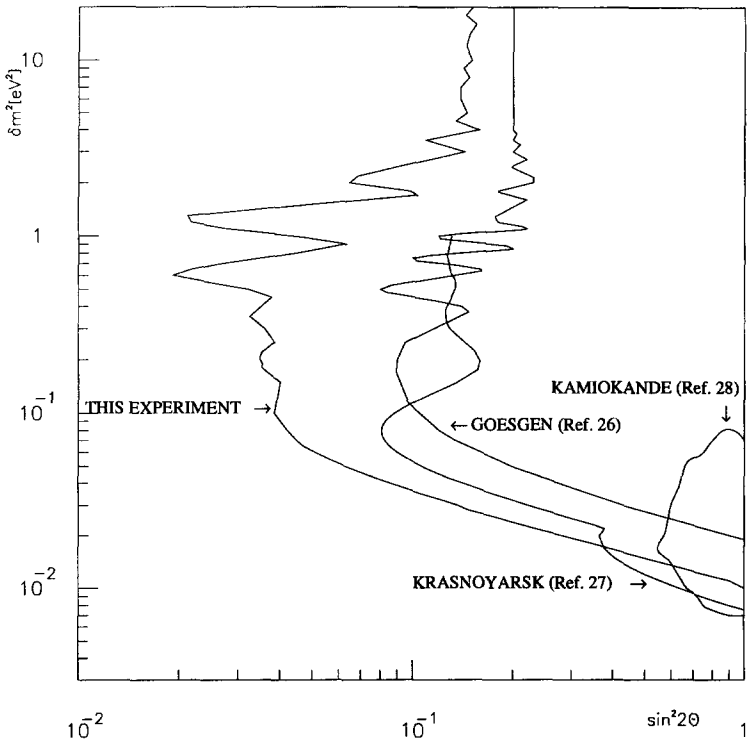


Fig. 18. The 90% C.L. exclusion contour obtained from the positron energy spectra measured at 40, 15 and 95 meters. Also shown is the hitherto excluded area in earlier reactor experiments with the region for a possible $\nu_e$–$\nu_\mu$ oscillation put forward by the KAMIOKANDE collaboration.

## 9. Conclusions

We have studied neutrino oscillations using a novel neutrino detection technique and increased significantly the statistics compared to all previous measurements on reactors. About 40% of the data were taken simultaneously at the two detection positions thereby reducing the systematic uncertainties due to burn-up. Comparing both the shapes and the integrated values of the positron spectra at 15 m, 40 m and 95 m distances we have been able to increase the exclusion region in the plane of the oscillation parameters with respect to previous experiments. Our high statistics measurement shows a very satisfactory agreement with the reactor spectrum deduced from the measured $\beta$-spectra for the main fuel components at ILL (Grenoble).

## Acknowledgements

This work has been supported by the Institute of Nuclear and Particle Physics (IN2P3-CNRS), the Commissariat à l'Energie Atomique (CEA-DSM-DAPNIA) and the French

Electricity Company (EdF).

S. Ait-Boubker, E. Aslanides, J. Berger, P. Besson, M. Poulet and B. Vignon took part in the early phase of the experiment, we thank them for their contributions.

We thank K. Schreckenbach for fruitful discussions on the systematic errors of the reactor spectra and for the access to their data taken at the ILL.

We are grateful to the staff of the Bugey nuclear power plant for their hospitality and help. The support of the technical staff of the participating laboratories, in particular that of M. Abbes, J. Ballansat, Ch. Barnoux, R. Bazzoli, M. Bermond, M. Billault, J. Boucher, M. Bouriant, B. Camberlin, M. Commerçon, Ph. Charvin, G. Daguin-Moynot, Th. Desanlis, J-M. Dubois, G. Farrache, Y. Gally, L. Giacobone, B. Guerre-Chaley, J-P. Jobez, D. Jourde, F. Léon, A. Menthe, J. Mullié, P. Ollive, A. Oriboni, J. Poinsignon, R. Potheau, R. Provasi [4], J. Thion and J-F. Thomas [5] is greatly acknowledged.

## References

[1] S.L. Glashow, Nucl. Phys. 22 (1987) 440;
S.Weinberg, Phys. Rev. Lett. 19 (1967) 1264;
A.Salam, *in* Elementary particle theory, ed. N. Svartholm (Almqvist and Wiksell, Stockholm, 1968) p. 367.

[2] See e.g. B. Kayser, The Physics of Massive Neutrinos (World Scientific, Singapore, 1989).

[3] J.F. Cavaignac et al., Phys. Lett. B 148 (1984) 387.

[4] M. Talby, Proc. XXVIth Int. Conf. on High Energy Physics, Munich 1989, ed. R. Kotthaus, J. Kühn (Springer Verlag, Berlin-Heidelberg, 1989), p. 1072;
M.Talby, Recherche des oscillations neutrinos auprès d'un réacteur. Thèse de doctorat d'Etat pour obtenir le titre de Docteur d'Etat-Sciences, Marseille, 1988; Proc. XXIIth Rencontre de Moriond, The Standard Model, the Supernova 1987A, ed. J. Tran Tan Vanh (Editions Frontières, 1987) p. 393.
H. de Kerret, Proc. XXIIIth Rencontre de Moriond, The 5th Force, Neutrino Physics, ed. J. Tran Tan Vanh (Editions Frontières, 1988) p. 125.

[5] B. Achkar et al., Contribution to the Joint Int. Lepton-Photon Symposium and Europhysics Conf. Geneva, Switzerland, July, 1991, quoted in the Proceedings of the Conference, p. 620.

[6] E. Kajfasz, Proc. XXVIIth Rencontre de Moriond, Progress in Atomic Physics, Neutrinos and Gravitation, ed. G. Chardin, O. Fackler and J. Tran Tanh Van (Editions Frontières, Gif-sur-Yvette, 1992) p. 145.

[7] NE320, produced by Nuclear Enterprise, Edinburg, U.K.

[8] B. Achkar et al., A liquid scintillator detector to study neutrino oscillation at the BUGEY nuclear power plant. (In preparation, to be submitted to Nucl. Instrum. Methods.)

[9] S. Ait-Boubker et al., Nucl. Instrum. Methods A277 (1989) 461.

[10] A. Stutz, Conception par simulation et réalisation d'un détecteur d'antineutrinos, Thèse pour obtenir le titre de Docteur de l'Université Joseph Fourier - Grenoble I, ISN Grenoble, 1989.

[11] R. Aleksan et al., Nucl. Instrum. Methods A 273 (1988) 303.

[12] Private communication of the reactor control group of the EDF (Electricité de France) on the Bugey site.

[13] P. Besson, Controle à court et long terme des gains d'un ensemble de photomultiplicateurs à l'aide d'un générateur de lumière et d'un système de distribution par fibres optiques, Thèse pour obtenir le titre de docteur es sciences, Annecy, 1989.
J. Berger et al., Nucl. Instrum. Methods, A 279 (1989) 343.

[14] B. Achkar, Recherche d'oscillations de neutrinos auprès d'un réacteur nucléaire, Thèse pour obtenir le titre de Docteur de l'Université Joseph Fourier - Grenoble I, ISN 92.100, Grenoble, 1992.

[4] Deceased.

[5] Deceased.

[15] F. Garciaz, Recherche des oscillations de neutrinos auprès d'un réacteur nucléaire, Thèse pour obtenir le titre de Docteur de l'Université de Provence, Marseille, 1992.
[16] K. Schreckenbach et al., Phys. Lett. B 160 (1985) 325;
A.A. Hahn et al., Phys. Lett. B 218 (1989) 365.
[17] H.V. Klapdor and J. Metzinger, Private communication.
[18] P. Vogel, Phys. Rev. D 29 (1984) 1918.
[19] H. de Kerret, B. Lefièvre, Simulation des neutrons de basse énergie par Monte Carlo, Collège de France, LPC 88-01.
[20] R. Brun et al., GEANT simulation package, Long Writeup, CERN Program Library W5013.
[21] V. McLane, Ch. L. Dunford and Ph. F. Rose, Neutron Cross Sections (Academic Press, New York, 1988)
[22] Y. Dufour, Comparaison entre la simulation et les premières données de Bugey III, Thèse pour obtenir le grade de Docteur ès Sciences Physiques, LPC T 89 01, Paris, 1989.
[23] J-P. Cussonneau, Comparaison entre la simulation et les données de neutrinos dans BUGEY 3, Thèse pour obtenir le titre de Docteur en Sciences Physiques, LPC 92T1, Paris, 1992.
[24] Review of Particle Properties, Phys. Rev. D 45 (June 1992)
[25] H. Yamaguchi, Prog. Theor. Phys. 23 (1960) 1117;
D.H. Wilkinson, Nucl. Phys. A 377 (1982) 474.
[26] G. Zacek et al., Phys. Rev. D 34 (1986) 2621
[27] G.S. Vidyakin et al., JETP Lett. 59 (1994) 364.
[28] Y. Fukuda et al., Phys. Lett. B 335 (1994) 237.
[29] K. Schreckenbach, Private communication;
J. Favier, Bugey Internal Note.